
Aachen Institute for Advanced Study in Computational Engineering Science

Preprint: AICES-2009-19

03/November/2009

Analysis of forward and inverse models in fluorescence
optical tomography

Herbert Egger, Manuel Freiberger and Matthias Schlottbom

Financial support from the Deutsche Forschungsgemeinschaft (German Research Association) through grant GSC 111 is gratefully acknowledged.

©Herbert Egger, Manuel Freiberger and Matthias Schlottbom 2009. All rights reserved

List of AICES technical reports: <http://www.aices.rwth-aachen.de/preprints>

Analysis of forward and inverse models in fluorescence optical tomography

Herbert Egger^a, Manuel Freiberger^b and Matthias Schlottbom^c

^aInstitute for Numerical Mathematics, TU Graz, Steyrergasse 30, 8010 Graz, Austria (corresponding author); email: eggerhe@gmail.com

^bInstitute of Medical Engineering, TU Graz, Kronesgasse 5/II, 8010 Graz, Austria; email: manuel.freiberger@tugraz.at

^cAachen Institute for Advanced Study in Computational Engineering Science, RWTH Aachen, Schinkelstraße 2, 52062 Aachen, Germany; email: schlottbom@aices.rwth-aachen.de

Abstract

This paper investigates forward and inverse problems in fluorescence optical tomography, with the aim to devise stable methods for the tomographic reconstruction.

We analyze solvability of a standard forward model and two approximations by reduced models, which provide certain advantages for a theoretical as well as numerical treatment of the inverse problem. Important properties of the forward operators, that map the unknown fluorophore concentration on virtual measurements, are derived; in particular, the ill-posedness of the reconstruction problem is proved, and the non-uniqueness is discussed.

For the stable reconstruction, we consider Tikhonov-type regularization methods, and we prove that the forward operators have all the properties, that allow to apply standard regularization theory. We also investigate the applicability of nonlinear regularization methods, i.e., TV-regularization and a method of levelset-type, which are better suited for the reconstruction of localized or piecewise constant solutions.

The theoretical results are supported numerical tests, which demonstrate the viability of the reduced models for the treatment of the inverse problem, and the advantages of nonlinear regularization methods for reconstructing localized fluorophore distributions.

1 Introduction

Diffuse optical tomography utilizes near-infrared light at wavelengths of 700-900nm to probe highly scattering media and determine distributed optical parameters from measurements of attenuated and scattered light intensities [37, 4]. Knowledge of absorption and scattering coefficients then allows to classify different materials, e.g., to distinguish between healthy tissue and cancer, see [38]

or [31], and the references therein. The diffusive nature of light propagation in tissue limits the image resolution of optical prospection to some extent, but the fact that the absorption of near infrared light is influenced by hemoglobin or lipid concentration makes optical tomography an imaging modality that provides additional functional information about the investigated material [28].

In order to overcome the typically low contrast in optical parameters, that results in low signal to noise ratios, fluorescence enhanced optical tomography [25, 26] employs the presence of fluorescent dyes, which absorb and re-emit light at different wavelengths. This allows to clearly separate between excitation and emitted light, thus increasing the contrast substantially. Since fluorescent markers accumulate in certain regions and the activity of fluorophores is influenced by metabolic states or processes, localized observations allow to obtain not only anatomical images, but also to image physiological activity in biological systems [36]. Optical imaging with fluorescent contrast agents [35] has therefore been successfully used in several applications [26], e.g., for in-vivo imaging of tumors [29].

Besides time-resolved measurements [24], which require ultrashort laser pulses and high fidelity measurement setups, intensity modulated light is frequently used as excitation source, yielding frequency domain modalities [30, 27, 25], for which appropriate measurement devices are available [17].

The physical model of fluorescence optical tomography [29, 13] consists of: (A) diffusion of photons at excitation wavelength from sources at the boundary into the body; (B) absorption of part of the photons at the excitation wavelength by fluorophores and re-emission at a longer wavelength; (C) diffusion of the re-emitted photons through the body, and (D) measurement of light intensities leaving the body. The aim of tomographic reconstruction in fluorescence imaging is to determine fluorescence yield and/or lifetime distributions from boundary measurements of the emitted light [30, 25]. This inverse problem can be phrased as a parameter identification problem governed by a system of diffusion equations, and like similar problems in optical or impedance tomography, the inverse problem is severely ill-posed, hence only limited resolution of reconstructions can be expected.

Several methods for a stable reconstruction have been proposed in literature, mostly based on certain linearizations [30, 34, 27], but also approaches utilizing nonlinear forward models have been reported, e.g., [32, 22].

In this report, we start from the diffusion approximation as a forward model for light propagation, and we investigate two and three dimensional nonlinear forward problems, and their approximation by reduced models. After demonstrating the ill-posedness of the corresponding inverse problems, we derive basic properties of the forward operators that allow to apply regularization methods of Tikhonov type [11]. Since by appropriate placement of fluorescent dyes, fluorescence tomography has the ability to image localized inhomogeneities, we investigate the use of nonlinear regularization approaches that are suitable to incorporate such a-priori information; in particular, we study the applicability

of TV-regularization [1] and a related method of levelset type [16, 10]. The advantages of such nonlinear methods for the tomographic reconstruction are illustrated by numerical tests.

The manuscript is organized as follows: In the next section, we introduce the mathematical model for light propagation in fluorescence tomography, and discuss the approximation by reduced models, that facilitate the treatment of the corresponding inverse problems. In Section 3, we state the inverse problems in detail, demonstrate their ill-posedness, and shortly comment on unique solvability. We then derive important properties of the forward operators, and demonstrate the applicability of Tikhonov type regularization methods, in particular TV-regularization and a method of levelset type. In Section 5 we report on numerical tests that illustrate the viability of the model approximations and reveal the benefits of the nonlinear regularization approaches over standard Tikhonov regularization. Some conclusions are given in the final section.

2 Governing model and simplifications

The propagation of light in highly scattering (dense) media is typically modelled by the diffusion approximation, which is obtained as a first order approximation for the radiative transfer equation by moment methods [6, 4]. The physical quantity of the diffusion model is the time and space dependent radiance ϕ , i.e., the directionally averaged photon density. In a time harmonic (e.g. intensity modulated) regime, the radiance can be expressed as a product $\phi = \Phi e^{i\omega t}$ of the complex valued modulation envelope Φ and the time harmonic variation $e^{i\omega t}$ [25].

2.1 The nonlinear forward model

Let Φ_x, Φ_m denote complex envelopes (amplitudes) of the light at excitation and emission wavelengths λ_x, λ_m ; indices $i = x, m$ are used to distinguish between e(x)citation and e(m)ission. The governing mathematical model of fluorescence tomography is then given by [25, 22]

$$-\nabla \cdot (\kappa_x \nabla \Phi_x) + \mu_x \Phi_x = q \quad \text{in } \Omega \quad (1)$$

$$-\nabla \cdot (\kappa_m \nabla \Phi_m) + \mu_m \Phi_m = \gamma \Phi_x \quad \text{in } \Omega, \quad (2)$$

where $\Omega \in \mathbb{R}^d$, $d = 2, 3$ denotes the domain occupied by tissue. The system is complemented by Robin boundary conditions

$$\kappa_i \partial_n \Phi_i + \rho_i \Phi_i = 0, \quad \text{at } \partial\Omega \quad (3)$$

which model that no photons can enter the domain from the exterior. The coefficient ρ_i allows to take different refractive indices into account [6, 4].

Full model

In general, the photon diffusion and absorption coefficients κ_i, μ_i depend on

optical parameters of the tissue and the fluorophore in the following way:

$$\kappa_i = \frac{1}{d(\mu_{a,i} + \mu_{f,i} + \mu'_{s,i})}, \quad \mu_i = \mu_{a,i} + \mu_{f,i} + \frac{i\omega}{\nu}, \quad \gamma = \frac{\eta\mu_{f,x}}{1 - i\omega\tau}, \quad (4)$$

where $\mu_{a,i}$ denotes the photon absorption coefficient of the material at wavelength λ_i , and $\mu'_{s,i}$ is the reduced scattering coefficient [4]. The absorption coefficients $\mu_{f,i}$ can be linked to the fluorophore concentration, i.e., $\mu_{f,i} = \epsilon_i c_f$ where c_f denotes the concentration of the fluorescent marker, and ϵ_i is a specific extinction coefficient. Finally, η and τ denote the fluorophore's quantum efficiency and lifetime, and ω, ν denote the modulation frequency and the speed of light, respectively. A detailed derivation and further references can be found in [13, 25, 22].

Throughout this presentation, we assume that the coefficients (except the fluorophore concentration when dealing with the inverse problem) are known but may depend on the spatial position in general. To ensure solvability of the model, we make the following assumptions.

- Assumption 1.** (i) $\Omega \subset \mathbb{R}^d$, $d = 2, 3$ is a simply connected Lipschitz domain.
(ii) The coefficients $\mu_{a,i}, \mu'_{s,i} \in L^\infty(\Omega)$ are non-negative, and $\mu_{a,i} + \mu'_{s,i}$ is uniformly positive, i.e., there exists a constant $\underline{\mu} > 0$ s.t. $\mu_{a,i} + \mu'_{s,i} \geq \underline{\mu}$ on Ω .
(iii) The functions $\epsilon_i, \eta, \tau \in L^\infty(\Omega)$ are non-negative, moreover ϵ_i and η_i are uniformly bounded from below away from zero.
(iv) The parameters $\rho_i \in L^\infty(\Omega)$ are uniformly greater than zero.
(v) The modulation frequency ω is an arbitrary real constant.

Under these assumptions, unique solvability of the system (1)–(3) is ensured.

Proposition 2. Let Assumption 1 hold. Then for any source $q \in H^1(\Omega)'$ and any non-negative $c_f \in L^\infty(\Omega)$, the system (1)–(4) has unique complex valued solutions $\Phi_x, \Phi_m \in H^1(\Omega)$ that satisfy the a-priori estimate

$$\|\Phi_x\|_{H^1} \leq C\|q\|_{(H^1)'}, \quad \|\Phi_m\|_{H^1} \leq C\|c_f\|_{L^{3/2}}\|q\|_{(H^1)'},$$

where the constant C depends only on the domain Ω and the bounds on the coefficients.

Proof. Under Assumption 1 on the coefficients and the condition on c , we obtain boundedness and uniform positivity of κ_i ; moreover $|\mu_i|$ is bounded from above and $\text{Re}(\mu_i) \geq 0$. Since ρ is uniformly positive, Poincaré's inequality then yields the coercivity of the associated sesquilinearforms, and unique solvability and the first estimate follow from the Lax-Milgram theorem [9, Theorem IV.1.1]. To obtain the second bound, note that by continuity of the Sobolev embedding [2] of $H^1(\Omega) \rightarrow L^p(\Omega)$ for all $p \leq 6$ (in 2 or 3 space dimensions), there holds

$$\|\gamma\Phi_x\|_{(H^1)'} \leq C'\|\gamma\Phi_x\|_{(L^6)'} \leq C''\left\|\frac{\eta\epsilon_x}{1 - i\tau\omega}\right\|_{L^\infty}\|c\|_{L^{3/2}}\|\Phi_x\|_{L^6},$$

which together with $\|\Phi_x\|_{L^6} \leq C'''\|\Phi_x\|_{H^1}$ (Sobolev embedding) and the first bound completes the proof. \square

2.2 Reduced models

Since in practice, the concentration c_f is typically small, one is tempted to neglect the contribution of the fluorophore to the absorption and/or diffusion coefficients. We will particularly consider the following two cases:

Partially reduced model

Neglecting the influence of the fluorophore on the coefficient κ_i yields

$$\kappa_i = \frac{1}{d(\mu_{a,i} + \mu'_{s,i})}, \quad \mu_i = \mu_{a,i} + \mu_{f,i} + \frac{i\omega}{\nu}, \quad \gamma = \frac{\eta\epsilon_x}{1 - i\omega\tau}c_f. \quad (5)$$

Fully reduced model

If the influence of the fluorophore on both parameters is neglected, we obtain

$$\kappa_i = \frac{1}{d(\mu_{a,i} + \mu'_{s,i})}, \quad \mu_i = \mu_{a,i} + \frac{i\omega}{\nu}, \quad \gamma = \frac{\eta\epsilon_x}{1 - i\omega\tau}c_f. \quad (6)$$

Remark 3. The fully reduced problem (1)–(3) with coefficients (6) yields a first order Born approximation for the full model, see [30, 27]. In this case, the excitation field Φ_x is completely independent of the fluorophore concentration c_f . The choice (5) for the coefficients yields a somewhat better approximation. Both reductions will facilitate the treatment of the inverse problem below.

The solvability of the reduced models follows with slight changes from Proposition 2, so we state it without proof.

Corollary 4. *Let Assumption 1 hold. Then for any $q \in H^1(\Omega)'$ and for any non-negative $c_f \in L^\infty(\Omega)$, the reduced problems (1)–(3) with coefficient (5) or (6) have unique solutions $\widehat{\Phi}_x, \widehat{\Phi}_m \in H^1(\Omega)$, which satisfy the estimates*

$$\|\widehat{\Phi}_x\|_{H^1} \leq C\|q\|_{(H^1)'}, \quad \|\widehat{\Phi}_m\|_{H^1} \leq C\|c_f\|_{L^{3/2}}\|q\|_{(H^1)'},$$

with constant C only depending on the domain and the bounds of the coefficients.

In order to quantify the perturbation introduced by the approximation of the coefficients κ_i and μ_i , we estimate the model error as follows.

Proposition 5. *Let Assumption 1 hold, and $\Phi_i, \widehat{\Phi}_i$ denote the solutions of (1)–(3) with coefficients (4) and (5), respectively. For $q \in H^1(\Omega)'$ and any non-negative $c_f \in L^\infty(\Omega)$, the difference in the solutions can be estimated by*

$$\|\Phi_x - \widehat{\Phi}_x\|_{H^1} \leq C\|c_f\|_{L^{3/2}}\|q\|_{(H^1)'}, \quad \|\Phi_m - \widehat{\Phi}_m\|_{H^1} \leq C\|c_f\|_{L^{3/2}}^2\|q\|_{(H^1)'}$$

If the coefficients in the equations for $\widehat{\Phi}_i$ satisfy (6) instead of (5), then the (weaker) estimates

$$\|\Phi_x - \widehat{\Phi}_x\|_{H^1} \leq C\|c_f\|_{L^\infty}\|q\|_{(H^1)'}, \quad \|\Phi_m - \widehat{\Phi}_m\|_{H^1} \leq C\|c_f\|_{L^{3/2}}\|c\|_{L^\infty}\|q\|_{(H^1)'}$$

hold.

Proof. We only proof the second estimate in detail. Let κ_i, μ_i denote the coefficients of (4) and $\widehat{\kappa}_i, \widehat{\mu}_i$ be defined according to (6). Furthermore, let Φ_i and $\widehat{\Phi}_i$ denote the corresponding solutions of (1)–(3), and define $w_x := \Phi_x - \widehat{\Phi}_x$ and $\delta\kappa_x := \kappa_x - \widehat{\kappa}_x, \delta\mu_x := \mu_x - \widehat{\mu}_x$. By linearity of the system (1)–(3), w_x solves

$$\begin{aligned} -\nabla \cdot (\widehat{\kappa}_x \nabla w_x) + \widehat{\mu}_x w_x &= \nabla \cdot (\delta\kappa_x \nabla \Phi_x) - \delta\mu_x \Phi_x && \text{in } \Omega, \\ \widehat{\kappa}_x \partial_n w_x + \rho_x w_x &= -\delta\kappa_x \partial_n \Phi_x && \text{on } \partial\Omega. \end{aligned}$$

Applying Corollary 4 and the Cauchy-Schwarz inequality, we obtain the bound $\|w\|_{H^1} \leq C(\|\delta\kappa_x\|_{L^\infty} + \|\delta\mu_x\|_{L^\infty})\|\Phi_x\|_{H^1}$. The first part of the second estimate then follows by the uniform bound on $\|\Phi_x\|_{H^1}$ (Proposition 2), and by estimating the differences in the parameters by $\|c_f\|_{L^\infty}$. The other estimates follow in a similar fashion. \square

Remark 6. Recalling that $\|\Phi_x\|_{H^1} = O(1)$ and $\|\Phi_m\|_{H^1} = O(\|c_f\|_{L^{3/2}})$, we conclude that the approximation of both fields is accurate to first order in $\|c_f\|_{L^{2/3}}$ respectively $\|c_f\|_{L^\infty}$ for the partly and fully reduced model.

2.3 Measurements and direct problems

The forward problem of fluorescence tomography is to determine the complex amplitudes Φ_x, Φ_m for a given distribution of the fluorophore and a prescribed set of excitations. All other coefficients appearing in (4) are assumed to be known. The measurable quantity, i.e. phase and intensity of the emitted light at wavelength λ_m on the boundary, can be defined by [4]

$$m = \kappa \partial_n \Phi_m = -\rho_m \Phi_m \quad \text{on } \partial\Omega. \quad (7)$$

Motivated by the requirements of Proposition 2 and Corollary 4, we consider the following set of admissible fluorophore concentrations

$$C_{ad} := \{c_f \in L^2(\Omega) : 0 \leq c_f \leq \overline{c}_f\} \subset L^2(\Omega).$$

Remark 7. The boundedness of fluorophore concentrations is a technical assumption that has to be made to ensure uniform positivity of the diffusion coefficient κ_i in (4) and thus guarantee uniform ellipticity and solvability of the system (1)–(3). Since the fluorophore distribution in tissue is typically governed by some diffusion process, this is a physically reasonable condition.

For a given excitation q , the mathematical forward models assign to some prescribed fluorophore concentration c_f the corresponding measurement m of the emitted light at the boundary. Solving this forward problem can be formulated as the action of a *forward operator*

$$F : C_{ad} \subset L^2(\Omega) \rightarrow L^2(\partial\Omega), \quad c \mapsto m. \quad (8)$$

Note that the definition of the forward operator can easily be generalized to the case of multiple sources; we will use the symbols F_q, m_q in that case to emphasize the dependence on the source q .

Remark 8. While the full and partially reduced forward models with coefficients (4) or (5) yield nonlinear forward operators, the forward operator of the reduced model (6) is in fact linear, i.e., $w := \widehat{\Phi}_m(c_1) - \widehat{\Phi}_m(c_2)$ solves (1)–(3) with c_f replaced by $c_1 - c_2$ in the definition (6) of γ . As we will see, this facilitates the theoretical and numerical treatment of the corresponding inverse problem considerably.

3 Inverse problem

The aim of fluorescence optical tomography is to determine an a-priori unknown fluorophore concentration c_f from measurements of the emitted light m . For a single excitation, this amounts to solving the operator equation

$$F(c_f) = m \quad c_f \in C_{ad}, \quad m \in L^2(\partial\Omega). \quad (9)$$

For ease of presentation, we only treat the case of a single excitation in detail. The results, however, generalize directly to multiple excitations, in which case the inverse problem might be stated as $F_q(c_f) = m_q$ for all excitations q .

As far as possible, we try to address the full and reduced models in a unified manner. So, the results given below hold likewise for the full and the reduced forward models, if not stated otherwise.

3.1 Compactness and ill-posedness

The ill-posedness of the inverse problem of fluorescence tomography follows directly from the following properties of the forward operator F .

Proposition 9. *The operator $F : C_{ad} \subset L^2(\Omega) \rightarrow L^2(\partial\Omega)$ is continuous and compact, i.e., it is completely continuous.*

Proof. Let $c^{(n)} \in C_{ad}$ converge in L^2 to some c ; since C_{ad} is a closed subset of $L^2(\Omega)$, it follows that $c \in C_{ad}$ as well. By Proposition 2 respectively Corollary 4, the corresponding solutions $\Phi_i^{(n)}$, Φ_i of (1)–(3) are uniformly bounded, i.e., $\|\Phi_i^{(n)}\|_{H^1} \leq C\|q\|_{(H^1)'}$ for all n . By the weak compactness of bounded sets in Hilbert spaces, there exist weakly convergent subsequences, again denoted by $\Phi_i^{(n)}$, that converge (weakly) to some $y_i \in H^1(\Omega)$. We will show that $y_x = \Phi_x$ (the corresponding result for the emitting field follows in the same way). Let $w_x^{(n)} := \Phi_x^{(n)} - \Phi_x$, then for every $v \in H^1(\Omega)$ there holds

$$\begin{aligned} & \int_{\Omega} \kappa_x \nabla w_x^{(n)} \nabla v + \mu_x w_x^{(n)} v \, dx + \int_{\partial\Omega} \rho_x w_x^{(n)} v \, ds \\ &= - \int_{\Omega} (\kappa_x^n - \kappa_x) \nabla \Phi_x^{(n)} \nabla v + (\mu_x^{(n)} - \mu_x) \Phi_x^{(n)} v \, dx. \end{aligned}$$

Since the right hand side converges to zero for all $v \in H^1(\Omega)$, and $w_x^{(n)} \rightharpoonup y_x - \Phi_x$, it follows from the unique solvability of the problem (1)–(3) that $y_x = \Phi_x$.

The result for the emitting field follows with similar arguments. By continuity of the trace mapping $H^1(\Omega) \rightarrow H^{1/2}(\partial\Omega)$ and the compact embedding $H^s(\partial\Omega) \hookrightarrow L^2(\partial\Omega)$ for $s > 0$ [2], we obtain that $\Phi_m^{(n)} \rightarrow \Phi_m$ (strongly) in $L^2(\partial\Omega)$. Finally, the compactness follows, since C_{ad} is mapped onto bounded sets in $H^{1/2}(\partial\Omega)$, which are precompact subsets of $L^2(\partial\Omega)$. \square

Remark 10. An inspection of the proof reveals, that F is also continuous with respect to the norms of $L^{3/2}(\Omega)$ and $L^2(\partial\Omega)$, which we will use later.

The compactness of the forward operators immediately implies the ill-posedness of the corresponding inverse problems.

Corollary 11. *Let $F : C_{ad} \subset L^2(\Omega) \rightarrow L^2(\partial\Omega)$. Then for either of the forward models, the inverse problem (9) is locally ill-posed [19], i.e., the solutions depend unstably on perturbations of the data.*

In order to apply standard results from regularization theory for the solution of the inverse problems, in particular to ensure existence of minimizers for regularized least-squares functionals, we require additional properties of the forward operators.

Proposition 12. *For the reduced models (1)–(3) with coefficients (5) or (6), the operator $F : C_{ad} \subset L^2(\Omega) \rightarrow L^2(\partial\Omega)$ is weakly sequentially closed.*

Proof. We only treat the partially reduced model (5) in detail. Let $c^{(n)} \in C_{ad}$, then $c^{(n)} \rightharpoonup c$ (weakly) in $L^2(\Omega)$. Since C_{ad} is a closed convex subset of $L^2(\Omega)$, it is weakly closed, and thus $c \in C_{ad}$. As in the proof of Proposition 9, we can extract subsequences of the corresponding solutions $\Phi_i^{(n)}$ of (1)–(3) that converge weakly in H^1 to some $y_i \in H^1(\Omega)$. We will show that $y_i = \Phi_i$, and again, we only treat the excitation fields $i = x$ in detail. The difference $w^{(n)} := \Phi_x^{(n)} - \Phi_x$ satisfies for any $v \in H^1(\Omega)$

$$\int_{\Omega} \kappa_x \nabla w^{(n)} \nabla v + \mu_x w^{(n)} v \, dx + \int_{\partial\Omega} \rho_x w^{(n)} v \, ds = - \int_{\Omega} (\mu_x^{(n)} - \mu_x) \Phi_x^{(n)} v \, dx.$$

By the compact embedding of $H^1(\Omega) \rightarrow L^p(\Omega)$, $p < 2d/(d-2)$ weak convergence in H^1 implies strong convergence in L^4 in both 2 and 3 space dimensions. This shows that the right hand side converges to zero for any $v \in H^1(\Omega)$. Recalling that $w_n \rightharpoonup y_x - \Phi_x$ weakly in L^2 , and using the unique solvability of (1)–(3), we conclude that $y_x = \Phi_x$, i.e., $\Phi_x^{(n)} \rightharpoonup \Phi_x$ weakly in H^1 , and by compact embedding of Sobolev spaces $\Phi_x^{(n)} \rightarrow \Phi_x$ strongly in L^p , $p < 2d/(d-2)$. The result for Φ_m follows in a similar way. The weak-closedness of F then finally follows from the continuity of the trace mapping. \square

Note that Proposition 12 cannot be generalized to the full forward model (4) directly. Utilizing the continuity of F , it is however possible to obtain weak-closedness with respect to a stronger topology in the parameter space.

Corollary 13. *For any of the forward models, the operator $F : C_{ad} \subset L^2(\Omega) \rightarrow L^2(\partial\Omega)$ is weakly sequentially closed with respect to the $H^1(\Omega)$ and $L^2(\partial\Omega)$ topologies.*

Proof. Let $c^{(n)} \in C_{ad}$ converge weakly in H^1 to some c . The compact embedding of $H^1(\Omega) \rightarrow L^2(\Omega)$ implies that $c^{(n)} \rightarrow c$ (strongly) in $L^2(\Omega)$, and the result follows from the continuity established in Proposition 9. \square

Remark 14. Since the trace mapping $H^1(\Omega) \rightarrow L^2(\partial\Omega)$ is compact, the proofs of the previous results show that the operator F in fact maps weakly convergent sequences into strongly convergent sequences.

3.2 A remark on uniqueness

Let us consider the fully reduced model (1)–(3) with parameters (6). In practice, the sources q are only located near the boundary, i.e., we may assume that there exists a domain $\tilde{\Omega} \subset \Omega$ whose closure is contained in Ω such that $\text{supp } q \subset \Omega \cap \tilde{\Omega}$. If we additionally assume that $\text{supp } c_f \subset \tilde{\Omega}$, then the inverse problem can be reduced to determine $f = \gamma\Phi_x$ in

$$\begin{aligned} -\nabla \cdot (\kappa_m \nabla \Phi_m) + \mu_m \Phi_m &= f && \text{in } \tilde{\Omega}, \\ \Phi_m &= g && \text{on } \partial\tilde{\Omega}, \end{aligned}$$

from (partial) knowledge of the Dirichlet-to-Neumann map $\Lambda_f : g \rightarrow \kappa_m \partial_n \Phi_m|_{\partial\tilde{\Omega}}$. Note, that for any function $v \in C_0^2(\tilde{\Omega})$ having compact support in $\tilde{\Omega}$, there holds

$$\Phi_m + v = \Phi_m, \quad \kappa_m \partial_n (\Phi_m + v) = \kappa_m \partial_n \Phi_m, \quad \text{on } \partial\tilde{\Omega},$$

and hence the problem with right hand side $\tilde{f} = f - \nabla \cdot (\kappa \nabla v) + \mu_m v$ has the same Dirichlet-to-Neumann map, i.e., $\Lambda_f = \Lambda_{\tilde{f}}$. This indicates that we cannot expect to obtain a unique solution for the inverse problem, at least for the fully reduced model, which is well known for related inverse potential problems [20]. Uniqueness results for similar source problems in potential theory do however hold, if the class of source functions f is restricted appropriately, e.g., if f is of the form $f = \bar{f}\chi_S$, where $S \subset \tilde{\Omega}$ is the support of f , χ_S is the characteristic function of the set S , and \bar{f} is some parameter. For details, we refer to [20].

4 Regularized solution

In order to cope with the ill-posedness of the inverse problem and the non-uniqueness of solutions, we consider Tikhonov-type regularization methods for an approximate but stable solution in this section. Motivated by the previous considerations on uniqueness respectively non-uniqueness, we will in particular investigate the use of nonlinear regularization terms that favour localized or piecewise constant solutions.

For ease of presentation, we again only consider the case of one excitation, but the results carry over verbatim to practically relevant case of multiple excitations.

4.1 Tikhonov regularization

As already shown in the previous section, the forward operator F is continuous and weakly sequentially closed. These properties allow to define regularized solutions c_α^δ as minimizers of the Tikhonov functional

$$J_\alpha^{L^2}(c; m^\delta) := \frac{1}{2} \|F(c) - m^\delta\|_{L^2(\partial\Omega)}^2 + \frac{\alpha}{2} \|c - c^*\|_{L^2(\Omega)}^2, \quad (10)$$

where m^δ denotes (possibly perturbed) measurements of the emitted light (7) satisfying

$$\|m^\delta - m\| \leq \delta \quad (11)$$

for some noise level $\delta \geq 0$. Here m denotes the correct data corresponding to the true fluorophore concentration c_f .

4.1.1 Existence and convergence of minimizers

The following standard results establish the viability of Tikhonov regularization for the stable solution of the inverse problems under investigation. The proofs are standard and are omitted; for details, see [11, Chapter 10].

Proposition 15. *Let F denote the forward operator of either of the reduced models (1)–(3) with parameters (5) or (6). Then for any $\alpha > 0$, the Tikhonov functional (10) has a minimizer $c_\alpha^\delta \in C_{ad}$.*

Proposition 16. *Let m^{δ_n} denote a sequence of data with $\|m^{\delta_n} - m\| \leq \delta_n$, $\delta_n \rightarrow 0$, and $\alpha_n \sim \delta_n$. Then for either of the reduced forward models (5) or (6), the regularized solutions $c_{\alpha_n}^{\delta_n}$ have a convergent subsequence. Moreover, the limit of any converging subsequence is a solution (a c^* -minimum-norm solution) of the inverse problem (9).*

Note that the fully reduced forward model (1)–(3) with (6) results in a linear inverse problem, and thus the c^* -minimum-norm solution is unique in this case. This simplifies the convergence statement, i.e., the regularized solutions $c_{\alpha_n}^{\delta_n}$ converge to the (unique) c^* -minimum norm solutions in this case.

In order to ensure well-definedness of Tikhonov regularization for the full forward model (1)–(3) with parameters (4), we utilize a stronger norm for the regularization term and Corollary 13.

Corollary 17. *If the Tikhonov functional (10) is replaced by*

$$J_\alpha^{H^1}(c_f; m^\delta) := \frac{1}{2} \|F(c_f) - m^\delta\|_{L^2(\partial\Omega)}^2 + \frac{\alpha}{2} \|c_f - c^*\|_{H^1}^2,$$

then the results of Proposition 15 and 16 also hold for the forward model with parameters (4); here, convergence holds with respect to the $H^1(\Omega)$ norm.

4.1.2 Convergence rates for the reduced model

In order to derive quantitative estimates, differentiability of the forward operator as well as a source condition are required. For ease of presentation, we only consider the fully reduced model (6) in detail. Recall that the forward operator of the reduced model is linear, and thus the derivative $F'(c_f) : L^2(\Omega) \rightarrow L^2(\partial\Omega)$ is a well-defined compact operator which is defined by $F'(c_f)h = F(h)$. Since $F'(c_f)$ does not depend on c_f , we also write $F'h$ instead of $F'(c_f)h$ in the following. For formulating a source condition, we require the adjoint F'^* of this operator.

Lemma 18. *Let $F : C_{ad} \subset L^2(\Omega) \rightarrow L^2(\partial\Omega)$ denote the forward map associated with the fully reduced problem (1)–(3) with coefficients (6). Then F is linear and thus Fréchet differentiable, and the action of the adjoint (derivative) operator on an element $r \in L^2(\partial\Omega)$ is given by $F'^*r = \frac{\eta\epsilon_x}{1-i\omega\tau}\Phi_x\bar{w}_m$, where w_m solves the adjoint problem*

$$\begin{aligned} -\nabla \cdot (\kappa_m \nabla w_m) + \bar{\mu}_m w_m &= 0 && \text{in } \Omega \\ \kappa_m \partial_n w_m + \rho_m w_m &= \rho_m r && \text{on } \partial\Omega. \end{aligned}$$

Having the adjoint derivative at hand, we are able to formulate source conditions and apply the standard results from regularization theory.

Proposition 19. *Let c_f denote the c^* -minimum norm solution of the inverse problem (9) with reduced forward model (1)–(3) and (6). Moreover, assume that*

$$c_f = c^* + (F'^* F')^\nu v \quad \text{for some } \nu > 0 \quad \text{and some } v \in L^2(\Omega).$$

Then for all $0 < \nu \leq 1$ and for the parameter choice $\alpha \sim \delta^{\frac{2}{2\nu+1}}$ the estimate

$$\|c_f - c_\alpha^\delta\| \leq C\delta^{\frac{2\nu}{2\nu+1}}$$

holds. If the parameter α is chosen by the discrepancy principle

$$\alpha := \sup\{a > 0 : \|F(c_a^\delta) - m^\delta\| \leq \tau\delta\},$$

with some $\tau > 2\|F'\|$, then the same convergence rates hold for $\nu \leq 1/2$.

The proof follows with standard arguments, and is omitted; for details we refer to [11, Section 4].

Remark 20. Since the inverse problem for the fully reduced model is linear, one can apply other regularization methods, e.g. iterative methods, that yield optimal convergence rates for all $\nu > 0$.

Remark 21. Similar convergence rate results can be derived for the inverse problems using the partially reduced and the full forward model (using H^1 regularization), see [11, Theorem 10.4] for details.

Recall that according to the remarks of Section 3.2, we cannot expect to be able to reconstruct the unknown fluorophore concentration uniquely, and thus the minimum-norm solution in the previous results will depend on (A) the choice of the a-priori element c^* , and (B) on the norm that is used for regularization. In the following two sections, we will choose other nonlinear regularization terms, that favour localized or piecewise constant solutions, and thus allow to incorporate qualitative a-priori information of this kind.

4.2 TV regularization

Consider the Tikhonov functional with total variation (TV) regularization [1]

$$J_\alpha^{TV}(c; m^\delta) := \|F(c) - m^\delta\|_{L^2(\partial\Omega)}^2 + \alpha |c|_{TV}, \quad (12)$$

where $|\cdot|_{TV}$ denotes the TV-seminorm defined by duality as

$$|c|_{TV} := \sup_{v \in V} \int_{\Omega} c \nabla \cdot v \, dx,$$

with $V := \{v \in C_0^1(\Omega, \mathbb{R}^d) : |v(x)| \leq 1 \text{ for all } x \in \Omega\}$. For smooth functions, e.g., $c \in C^1(\overline{\Omega})$ there holds $|c|_{TV} = \int_{\Omega} |\nabla c| \, dx$. Let us also define the space of functions of *bounded variation* given by

$$BV(\Omega) := \{c \in L^1(\Omega) : |c|_{TV} < \infty\},$$

and recall that, equipped with the norm $\|\cdot\|_{BV} := \|\cdot\|_{L^1} + |\cdot|_{TV}$, the space $BV(\Omega)$ is a Banach space. For details on functions of bounded variation, and proofs of the following statements, we refer to [5, Section 2.2].

Lemma 22. *Let $\Omega \subset \mathbb{R}^d$ be a bounded open set. Then for $k \geq 0$, the sub-levelsets $S_k := \{c \in C_{ad} : |c|_{TV} \leq k\}$ are bounded compact subsets of $L^p(\Omega)$ for $1 \leq p < d/(d-1)$, i.e., any sequence $c^{(n)}$ in S_k has a subsequence that converges (strongly) in $L^p(\Omega)$.*

Lemma 23. *The bounded variation seminorm $|\cdot|_{TV} : BV(\Omega) \rightarrow \mathbb{R}$ is weakly lower semicontinuous, i.e., if a sequence $c^{(n)} \in BV(\Omega)$ converges (strongly) to some c with respect to the L^1 norm, then $|c|_{TV} \leq \liminf_n |c_n|_{TV}$.*

We are now able to show that the regularized solutions, defined as minimizers of (12), are well-defined.

Proposition 24. *Let F denote the operator to either of the forward models. Then for $\alpha > 0$, the functional (12) has a minimizer. For the fully reduced model with coefficients (6), the minimizer is unique.*

Proof. The proof uses standard arguments of the calculus of variations: for $\alpha > 0$ and k sufficiently large, the sub-levelsets $\{c \in C_{ad} : J_\alpha^{TV}(c; m^\delta) \leq k\}$ are compact in L^p , $p < d/(d-1)$, and thus the L^p -limit of a minimizing sequence exists in C_{ad} . Due to the weak-lower semicontinuity of the norms and the continuity of F as operator from $L^p(\Omega)$ to $L^2(\partial\Omega)$, $p \geq 3/2$ (see Remark 10),

the limit is a minimizer. Since the constant $c \equiv 1$ is not in the nullspace of the fully reduced (linear) forward operator, the functional J_α^{TV} is strictly convex in this case, which yields uniqueness of the minimizer. \square

With standard arguments one can show stability of the regularized solutions with respect to perturbations of the data m^δ or variations of the regularization parameter α ; see [1] for details. Moreover, convergence of the regularized solutions can be obtained, if the noise level tends to zero, and the regularization parameter is chosen appropriately.

Proposition 25. *Let m^{δ_n} denote a sequence of data such that $\|m^{\delta_n} - m\| \leq \delta_n$, and assume that $\delta_n \rightarrow 0$ and $\alpha_n \sim \delta_n$. Then the sequence of minimizers $c_{\alpha_n}^{\delta_n}$ has a convergent (strongly in L^p , $p < d/(d-1)$) subsequence, and the limit of every convergent subsequence is a solution of (9).*

Proof. The result follows with the same arguments as in the case of L^2 regularization. For the fully reduced (linear) model (6), the result corresponds to Theorem 5.1 in [1]. \square

Remark 26. For our numerical experiments, we utilize that the TV-seminorm $|\cdot|_{TV}$ can be approximated by a relaxed functional

$$R_\epsilon(c) := \int_\Omega \sqrt{\epsilon + |\nabla c|^2} dx,$$

where $\epsilon > 0$ ensures smoothness of the regularization term where $|\nabla c|$ vanishes. For details on this relaxation we refer to [1].

In the following, we outline a related method which allows to incorporate the additional a-priori information that the solution attains only certain values. Similar a-priori assumptions can be used to obtain uniqueness of solutions to related inverse problems in potential theory, see [20] and the remarks in Section 3.2.

4.3 A method of levelset type

In order to approximate solutions that are piecewise constant (or have steep gradients between areas of almost constant value), we adapt an approach that was proposed in [16]; see also [10]. To simplify the presentation, we consider only the case that the true solution c_f is binary valued, i.e., of the form

$$c_f = \chi_S, \quad S \subset \Omega, \tag{13}$$

where the set S is measurable and $\mathcal{H}^{d-1}(\partial S) < \infty$. Here, $\mathcal{H}^{d-1}(\partial S)$ denotes the $(d-1)$ -dimensional Hausdorff measure of the boundary ∂S , and χ_S is the characteristic function of a set S . In order to incorporate such a-priori information, the unknown fluorophore distribution is parameterized in the form

$$c = H_\epsilon(\phi), \tag{14}$$

where H_ϵ is some smooth, strictly monotonically increasing function converging pointwise to the Heaviside function, i.e., $H_\epsilon(x) \rightarrow H(x) := \chi_{\{x>0\}}$ with $\epsilon \rightarrow 0$ for any $x \in \mathbb{R}$. The function ϕ acts as a levelset function, i.e., the parameter $c = H_\epsilon(\phi)$ takes values close to one whenever ϕ is positive, and close to zero where ϕ is negative. In the limit case $\epsilon = 0$, the domain S is characterized by the levelsets $S = \{x : \phi(x) > 0\}$, see [16] for details. Similar as in the case of TV-regularization, the parameterization with $\epsilon > 0$ is a relaxation of the discontinuous case $\epsilon = 0$.

As a regularization method, we consider again a method of Tikhonov type, i.e., we define regularized solutions as minimizer of the functional

$$J_\alpha^{LS}(\phi; m^\delta) = \frac{1}{2} \|F(H_\epsilon(\phi)) - m^\delta\|^2 + \alpha(\beta \|H_\epsilon(\phi)\|_{TV} + \frac{1}{2} \|\phi - \phi^*\|_{H^1}^2). \quad (15)$$

By similar arguments as in the previous section, we obtain well-posedness of the regularized problems for the full as well as the reduced forward models; see [10, Section 2] for details and proofs.

Proposition 27. *For $\alpha > 0$, $\beta \geq 0$, and either of the forward models, the functional (15) has a minimizer. Moreover, for $\delta_n \rightarrow 0$ and $\alpha_n \sim \delta_n$, subsequences of regularized solutions converge to solutions of the inverse problem (9), i.e.,*

$$\|\phi_{\alpha_n}^{\delta_n} - \phi_f\|_{H^1} \rightarrow 0, \quad \|H_\epsilon(\phi_{\alpha_n}^{\delta_n}) - c_f\|_{H^1} \rightarrow 0,$$

where $c_f = H_\epsilon(\phi_f)$ is a solution of (9).

Remark 28. Note that the result holds for any $\beta \geq 0$, i.e., the TV-regularization term can be dropped as long as $\epsilon > 0$. We will take advantage of this fact in our numerical experiments. However, to obtain stability also for the limiting case $\epsilon = 0$, one has to set $\beta > 0$ and obtains convergence of solutions $H(\phi_{\alpha_n}^{\delta_n})$ only with respect to $L^p(\Omega)$, $p < d/(d-1)$, similarly as for TV-regularization. For details and proofs we refer to [16, 10]. For $\beta > 0$ or if one of the reduced models is considered, the H^1 -regularization term can be replaced by the L^2 -norm [10].

5 Numerical experiments

For illustration of the theoretical results derived so far, i.e., the approximability of the full forward model by reduced models, and the stabilized solution of the inverse problems by regularization methods of Tikhonov type, let us report on some results obtained in numerical test studies.

5.1 A test problem

For our numerical experiments, we consider the following two dimensional test problem: Ω is a disc with 30mm diameter, and 16 sources are placed on equally spaced intervals of 1mm length at the boundary. The measurements are taken

at 16 detectors of length 4mm, which are located between the locations of the excitation; see Figure 1 for a sketch of the geometry.

For the optical parameters at wavelengths $\lambda_x = 785\text{nm}$ and $\lambda_m = 830\text{nm}$, we use the following realistic values reported [3]: $\mu'_{s,x} = 0.275$, $\mu_{a,x} = 0.036$ and $\mu'_{s,m} = 0.235$, $\mu_{a,m} = 0.029$ at excitation respectively emission wavelength; all parameters are given in mm^{-1} . The molar extinction coefficients of the fluorophore were set to $\epsilon_x = 5 \cdot 10^4$ and $\epsilon_m = 5 \cdot 10^3$ in $\text{mm}^{-1}\text{mol}^{-1}$ [21]. For the remaining fluorophore parameters, we use $\eta = 0.016$ and $\tau = 0.56\text{ns}$; the modulation frequency is set to $\omega = 2\pi \times 10^8\text{s}^{-1}$ and we choose $\rho_x = \rho_m = 0.2$ [23].

As a test case, we choose a fluorophore distribution in form of a Gaussian peak with maximum concentration 1 [mol mm^{-3}] and width $\sigma = \sqrt{5}$ [mm]. The measurement setup and the initial fluorophore distribution are depicted in Figure 1.

5.2 Discretization by finite elements

The system (1)–(3) can be discretized by a finite element method using standard piecewise linear, continuous finite elements [7]. For approximating the fluorophore distribution c_f , we use the same continuous finite elements, which allows to apply H^1 - and TV -regularization easily. The discretization of the forward model (1)–(3) yields a complex linear system of the form

$$\begin{aligned} [K(\kappa_x) + M(\mu_x) + R(\rho_x)]P_x &= Q, \\ [K(\kappa_m) + M(\mu_m) + R(\rho_m)]P_m &= B(\gamma, P_x), \end{aligned}$$

where $K(\kappa)$, $M(\mu)$ denote the stiffness and mass matrices with coefficients κ and μ , and $R(\rho)$ is the matrix resulting from discretization of the Robin boundary terms. Q is a matrix whose 16 columns correspond to the discretization of the individual source terms, and $B(\gamma, P_x)$ is a matrix whose columns correspond to the corresponding right hand side of (2). The columns of the solution matrices P_x , P_m contain the discrete solutions of (1)–(3) for the different excitations.

The application of the discretized forward operator then consist in solving this linear system, and extracting the measurements $m = EP_m$, where E is an appropriate (measurement) matrix having 16 rows. The application of the discrete derivative $F'(c)h$ and its adjoint $F'^*(c)r$ can be realized via the solution of similar systems, see [15] for details.

5.3 Comparison of forward models

In the following, we report on results obtained with finite element simulations for the full model (4), and the reduced forward models (5) and (6). In particular, we compare the size of the perturbations introduced by the problem reduction (cf. Proposition 5) with the approximation error due to discretization.

For the simulation of the forward problems, we use meshes with 2052, 8208, 32832, 131328 and 525312 elements, respectively. As a reference solution we

take the solution of the full problem obtained on the finest mesh with 525 312 elements. In Table 1, we report the resulting residuals $\text{res} := \|m - m^{ref}\|/\|m^{ref}\|$, where the norm in the measurement space is defined simply by $\|m\|^2 := \sum_{ij} m_{ij}^2$; but one might as well use weighted norms for the measurements. For the prob-

elements	$\text{res}^{(A)}$	$\text{res}^{(B)}$	$\text{res}^{(C)}$
2 052	0.48078	0.46476	0.51296
8 208	0.20744	0.19485	0.23494
32 832	0.08563	0.07484	0.11121
131 328	0.02803	0.01994	0.05351
525 312	0.00000	0.01458	0.02722

Table 1: Relative errors $\text{res} := \|m - m^{ref}\|/\|m^{ref}\|$ in the output for the full (A), partially reduced (B), and fully reduced (C) forward models.

lem under investigation, the relative perturbation due to the use of the partially or fully reduced forward problems is in the order of 1–2%, and it is comparable to the error introduced by discretization up to meshes with more than 100 00 elements. This justifies the use of reduced forward models for the solution of the inverse problem.

Let us now report on some numerical tests concerning the regularized solution of the inverse problem.

5.4 Regularized reconstructions

In a second test study, we want to demonstrate the benefits from using nonlinear regularization methods that favour localized or strongly varying solutions for the reconstruction of localized fluorophore distributions. As in the previous tests, we utilize synthetic data, which are generated by solving the full forward model on the finest discretization. Motivated by the comparison of the forward models, we utilize the fully reduced forward model on a mesh with 32 832 elements for solving the inverse problem. This introduces model and approximation errors in the inverse problem, which will be present in a real experiment in any case, and prevents inverse crimes. The synthetic data are additionally perturbed by uniformly distributed random noise in the size of 0.1% of the data.

For the reconstruction, we use different regularization methods discussed in Section 4. The results of our numerical tests are displayed in Figure 1. The relative reconstruction errors $\text{err} = \|c^\dagger - c_\alpha^\delta\|_{L^2}/\|c^\dagger\|_{L^2}$ for the different methods are: 44% for the L^2 -regularization, 24% for the TV-regularization and 30% for the method of levelset-type. In order to obtain reconstruction errors of 25 – 30% for the L^2 -regularization, one would have use data with less than 0.01% noise; this reflects the severe ill-posedness of the problem. As the numerical results indicate, the reconstruction of localized solutions can therefore be enhanced considerably by utilizing nonlinear regularization terms instead of more standard linear terms like the L^2 - or H^1 -norm.

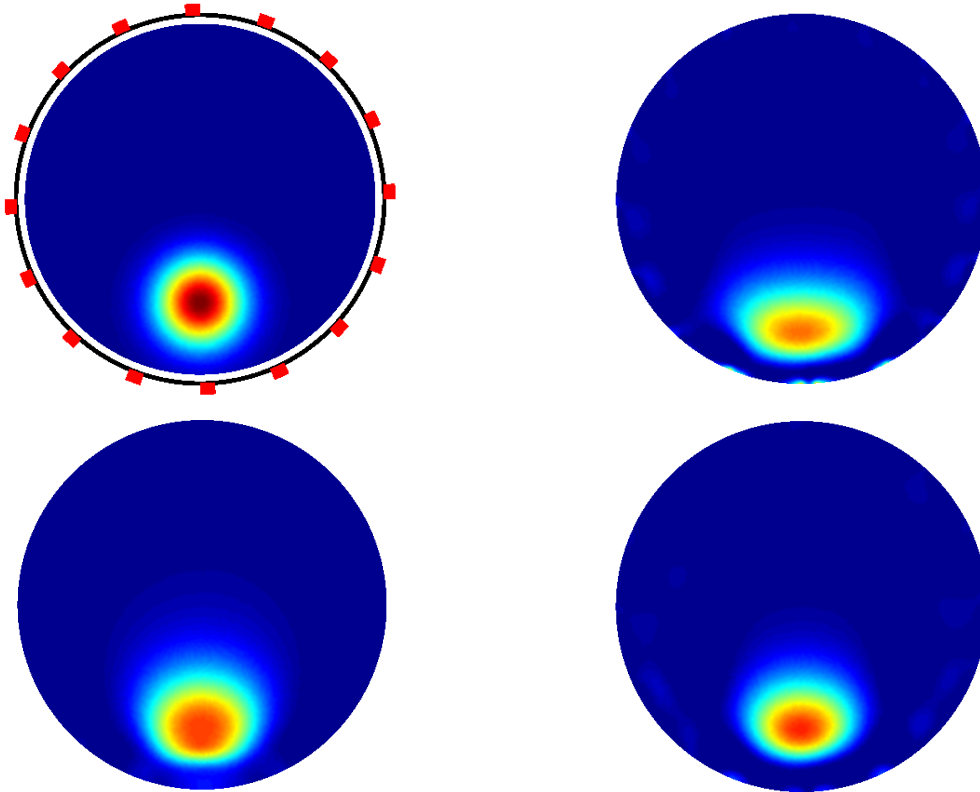


Figure 1: Setup and true parameter (top left): locations of the excitation in red, black bars denote the detector areas; reconstructions with L^2 -norm regularization (top right), TV-regularization (bottom left), and the levelset-type method (bottom right).

6 Summary

In this manuscript, we investigated different forward models for fluorescence diffuse optical tomography. In particular, we considered approximations of the full forward model by reduced models, and estimated the perturbations introduced by these model reductions.

The ill-posedness of the corresponding inverse problems follows from continuity and compactness of the forward operators, established in Section 3. As a comparison with related inverse problems in potential theory shows, uniqueness for the reconstruction of the fluorophore distribution cannot be expected, and therefore the incorporation of a-priori information into solution algorithms will have great influence on the quality of the reconstructions.

Important properties of the forward operators, that allow the application of standard result from regularization theory, could be established. In particular, the applicability of nonlinear regularization methods, that allow the incorpora-

tion of a-priori information about the solution, e.g., local support or piecewise constantness, has been investigated.

As the numerical results demonstrate, the model error introduced by relying on reduced forward models is relatively small in typical applications, and therefore reduced (linearized) models can be used for efficiently solving the inverse problem. Additionally, the reconstruction of localized solutions could be improved considerably, if appropriate nonlinear regularization methods, like TV-regularization, were used.

Acknowledgments

Support by Deutsche Forschungsgemeinschaft (DFG) through grant GSC 111 and the Austrian Science Foundation (FWF) through grant SFB/F32 is gratefully acknowledged.

References

- [1] R. Acar and C. R. Vogel. Analysis of bounded variation penalty methods for ill-posed problems. *Inverse Problems*, 10:1217–1229, 1994.
- [2] R. A. Adams. *Sobolev Spaces*. Academic Press, New York, San Francisco, London, 1975.
- [3] G. Alexandrakis, F. R. Rannou, and A. F. Chatziioannou. Tomographic bioluminescence imaging by use of a combined optical-pet (opet) system: a computer simulation feasibility study. *Phys. Med. Biol.*, 50:4225–4241, 2005.
- [4] S. R. Arridge. Optical tomography in medical imaging. *Inverse Problems*, 15:R41–R93, 1999.
- [5] G. Aubert and P. Kornprobst. *Mathematical problems in image processing*. Springer, New York, 2nd edition, 2006.
- [6] K. M. Case and P. F. Zweifel. *Linear Transport Theory*. Addison-Wesely Publishing Co., Reading, 1967.
- [7] P. Ciarlet. *The finite element method for elliptic problems*. North-Holland, Amsterdam, New York, 1978.
- [8] A. X. Cong and G. Wang. A finite-element-based reconstruction method for 3D fluorescence tomography. *Opt. Express*, 13:9847–9857, 2005.
- [9] D. E. Edmunds and W. D. Evans. *Spectral Theory and Differential Operators*. Oxford University Press, New York, 1987.
- [10] H. Egger and A. Leitão. Nonlinear regularization methods for ill-posed problems with piecewise constant or strongly varying solutions. *Inverse Problems*, 25:accepted, 2009.
- [11] H. W. Engl, M. Hanke, and A. Neubauer. *Regularization of Inverse Problems*. Kluwer, Dordrecht, 1996.

- [12] M. J. Eppstein, D. J. Hawrysz, A. Godavarty, and E. M. Sevick-Muraca. Three-dimensional, Bayesian image reconstruction from sparse and noisy data sets: Near-infrared fluorescence tomography. *PNAS*, 99:9619–9624, 2002.
- [13] T. J. Farrell and M. S. Patterson. Diffusion modeling of fluorescence in tissue. In M.-A. Mycek and B. W. Pogue, editors, *Handbook of Biomedical Fluorescence*, New York, Basel, 2003. Marcel Dekker Inc.
- [14] F. Fedele, J. P. Laible, and M. J. Eppstein. Coupled complex adjoint sensitivities for frequency-domain fluorescence tomography: theory and vectorized implementation. *J. Comput. Phys.*, 187:597–619, 2003.
- [15] M. Freiburger, H. Egger, and H. Scharfetter. Nonlinear regularization for fluorescence optical tomography. Technical Report NUMBER, Graz University of Technology, 2009.
- [16] F. Frühauf, O. Scherzer, and A. Leitão. Analysis of regularization methods for the solution of ill-posed problems involving discontinuous operators. *SIAM J. Numer. Anal.*, 43:767–786, 2005.
- [17] A. Godavarty, M. J. Eppstein, C. Zhang, S. Theru, A. B. Thompson, M. Gurfinkel, and E. M. Sevick-Muraca. Fluorescence-enhanced optical imaging in large tissue volumes using a gain-modulated ICCD camera. *Phys. Med. Biol.*, 48:1701–1720, 2003.
- [18] F. A. Grünbaum. Diffuse tomography: the isotropic case. *Inverse Problems*, 8:409–419, 1992.
- [19] B. Hofmann and O. Scherzer. Factors influencing the ill-posedness of nonlinear problems. *Inverse Problems*, 10, 1994.
- [20] V. Isakov. *Inverse source problems*. Number 34 in Mathematical Surveys and Monographs. American Mathematical Society, Providence, Rhode Island, 1992.
- [21] A. Joshi. *Adaptive finite element methods for fluorescence enhanced optical tomography*. PhD thesis, Texas A&M University, 2005.
- [22] A. Joshi, W. Bangerth, and W. M. Sevick-Muraca. Adaptive finite element based tomography for fluorescence optical imaging in tissue. *Opt. Express*, 12:5402–5417, 2004.
- [23] M. Keijzer, W. M. Star, and P. R. M. Storchi. Optical diffusion in layered media. *Applied Optics*, 27:1820–1824, 1988.
- [24] S. Lam, F. Lesagne, and X. Intes. Time domain fluorescent diffuse optical tomography: analytical expressions. *Opt. Express*, 13:2263–2275, 2005.
- [25] A. B. Milstein, S. Oh, K. J. Webb, C. A. Bouman, Q. Zhang, D. A. Boas, and R. P. Millane. Fluorescence optical diffusion tomography. *Appl. Opt.*, 42:3081–3094, 2003.
- [26] M.-A. Mycek and B. W. Pogue, editors. *Handbook of Biomedical Fluorescence*, New York, Basel, 2003. Marcel Dekker Inc.
- [27] V. Ntziachristos and R. Weissleder. Experimental three-dimensional fluorescence reconstruction of diffuse media by use of a normalized Born approximation. *Opt. Lett.*, 26:893–895, 2001.
- [28] V. Ntziachristos, A. Yodh, M. Schnall, and B. Chance. Concurrent MRI

- and diffuse optical tomography of breast after indocyanine green enhancement. *Proc. Natl. Acad. Sci.*, 97:2767–2772, 2000.
- [29] M. A. O’Leary, D. A. Boas, B. Chance, and A. G. Yodh. Reradiation and imaging of diffuse photon density waves using fluorescent inhomogeneities. *J. Lumin.*, 60&61:281–286, 1994.
- [30] M. A. O’Leary, D. A. Boas, X. D. Li, B. Chance, and Y. G. Yodh. Fluorescence lifetime imaging in turbid media. *Opt. Lett.*, 21:158–160, 1996.
- [31] B. C. R. R. and Alfano, editors. *Optical Tomography, Photon Migration, and Spectroscopy of Tissue and Model Media: Theory, Human Studies, and Instrumentation*, 1995. Proc. SPIE 2389.
- [32] R. Roy and E. M. Sevick-Muraca. Truncated Newton’s optimization scheme for absorption and fluorescence optical tomography: Part I theory and formulation. *Opt. Express*, 4:353–371, 1999.
- [33] R. Roy and E. M. Sevick-Muraca. Truncated Newton’s optimization scheme for absorption and fluorescence optical tomography: Part II reconstruction from synthetic measurements. *Opt. Express*, 4:372–382, 1999.
- [34] J. Schotland. Continuous wave diffusion imaging. *J. Opt. Soc. Am. A*, 14:275–279, 97.
- [35] E. M. Sevick-Muraca, A. Godavarty, J. P. Houston, A. B. Thompson, and R. Roy. Near-infrared imaging with fluorescent contrast agents. In M.-A. Mycek and B. W. Pogue, editors, *Handbook of Biomedical Fluorescence*, New York, Basel, 2003. Marcel Dekker Inc.
- [36] E. Shives, Y. Xu, and H. Jiang. Fluorescence lifetime tomography of turbid media based on an oxygen-sensitive dye. *Opt. Express*, 10:1557–1562, 2002.
- [37] J. Singer, F. A. Grünbaum, P. Kohn, and J. Zubelli. Image reconstruction of the interior of bodies that diffuse radiation. *Science*, 248:990–993, 1990.
- [38] B. J. Tromberg, N. Shah, R. Lanning, A. Cerussi, J. Espinozza, T. Pham, L. Svaasand, and J. Butler. Non-invasive in vivo characterization of breast tumors using photon migration spectroscopy. *Neoplasia*, 2:26–40, 2000.
- [39] D. Wang, X. Song, and J. Bai. Adaptive-mesh-based algorithm for fluorescence molecular tomography using an analytical solution. *Opt. Express*, 15:9722–9730, 2007.

